Available online at www.sciencedirect.com
SCIENCE DIRECT®
Journal of Power Sources 116 (2003) 174–184
JOURNAL OF POWER SOURCES
www.elsevier.com/locate/jpowsour

Impedance modeling of intermediate size lead–acid batteries

Alvin J. Salkind[a,d,*], Pritpal Singh[b], A. Cannone[a,d], Terrill Atwater[a,c], Xiquan Wang[e], David Reisner[e]

[a]*Center for Battery Materials and Engineering, School of Engineering, Rutgers University, The State University of New Jersey, 98 Brett Road, Piscataway, NJ 08854-8058, USA*
[b]*Villanova University, Villanova, PA 19085, USA*
[c]*US Army CECOM, RD&EC, Ft. Monmouth, NJ 07703, USA*
[d]*UMDNJ-Robert Wood Johnson Medical School, Piscataway, NJ 08854, USA*
[e]*US Nanocorp Inc., 74 Batterson Park Road, Farmington, CT 06032, USA*

Abstract

This presentation continues the study of the dynamic characteristics of lead–acid batteries previously reported into larger cells and batteries. Electrochemical impedance spectroscopy combined with fuzzy logic methodology of data analysis was used to characterize 6 V 10 Ah VRLA batteries and larger batteries used in tanks and other vehicles. Equivalent circuits were derived which can be used to estimate state-of-charge (SOC) and state-of-health.

Keywords: Lead–acid batteries; Electrochemical impedance spectroscopy; VRLA batteries; Modeling of battery equivalent circuits

1. Introduction and background

Modeling of lead–acid batteries based on impedance measurements has become very important recently with several groups reporting results in this area [1–4]. This paper represents the third discussion of results obtained in collaborative studies on lead–acid battery dynamics. The initial report [5] was presented in 1999 in Brighton, England. The second report was presented in 2001 [6]. Additional and previous results, by individual co-authors, have been reported in the literature [7–9], in academic theses, and in posters at ELBC meetings [10,11]. These earlier reports were mainly concerned with small VRLA type cells of 1–2.5 Ah capacity. In this study, we report on data from larger size cells and batteries, in multi-cell battery stacks, and on batteries used in Army tanks.

In the previous studies, effects of cell/battery orientation position on performance were discussed as well as the effects of separator type and compression. To enable data collection and increase the understanding of individual electrode dynamics, commercial size VRLA batteries (6 V, 10 Ah) were modified by the insertion of reference electrodes. This size was chosen since it is widely used in many applications, including tools, emergency lighting, and electrical and medical devices. In addition, work was continued with the D-size cells previously discussed, but in a battery array. This provided an ability to compare single cell data with multi-cell batteries using the same cell design.

The tank type battery is not a VRLA design, but is typical of large traction and SLI batteries used in trucks and traction units, both on-road and off-road. Data on this design represented a major scale-up in the modeling activity and provided a good test of the scalability of the previous modeling.

The modeling and performance prediction of lead–acid batteries has to consider effects of cycling, design, electrode active material ratios, electrolyte type and amount, and operating temperature. The ac impedance methods of studying the electrochemical dynamics, combined with a fuzzy logic methodology for data interpretation, seem to offer an effective method for understanding system dynamics and providing a useful tool that can be used in a low cost system analyzer.

2. Experimental

The two batteries upon which measurements were made were the Yuasa NP 10-6 6 V 10 Ah batteries (see Fig. 1a) and the Exide (US) US6TMF military batteries (see Fig. 1b).

* Corresponding author. Tel.: +1-732-445-6858; fax: +1-732-445-1669.
E-mail address: salkind@rci.rutgers.edu (A.J. Salkind).

0378-7753/03/$ – see front matter
doi:10.1016/S0378-7753(02)00690-0

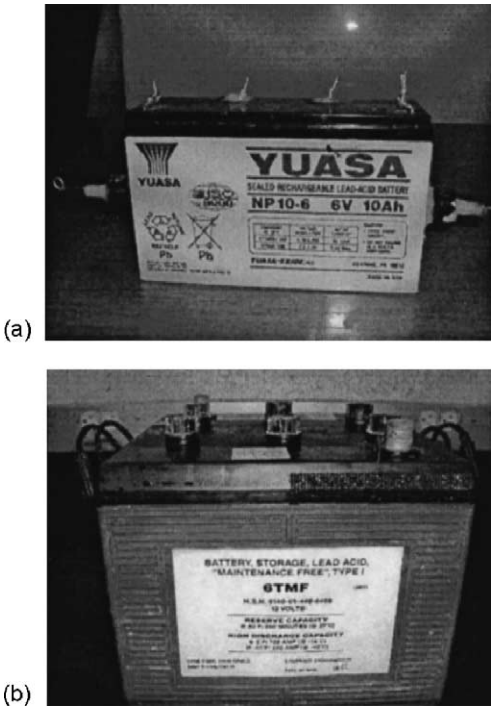

Fig. 1. (a) Picture of Yuasa NP 10-6 6 V 10 Ah battery; (b) picture of Exide Military US6TMF 12 V 100 Ah battery. Battery specifications are—nominal voltage: 6 V; nominal capacity: 20 h rate of 500 mA to 5.25 V 10.0 Ah; 10 h rate of 930 mA to 5.25 V 9.3 Ah; 5 h rate of 1700 mA to 5.10 V 8.5 Ah; 1 h rate of 6000 mA to 4.80 V 6.0 Ah; weight (approximately): 4.41 lb (2.0 kg); internal resistance of charge: 10 mΩ (approximately); charge methods (at 20 °C): cycle use—maximum charging current 2.5 A and charging voltage 7.2–7.5 V, standby use—float charging voltage 6.75–6.90 V.

Some of the specifications for the YUASA sealed rechargeable lead–acid.

The battery was modified by inserting two $Hg{\cdot}Hg_2SO_4$ reference electrodes. The electrodes were inserted through the sidewalls of the two external cells of the three-cell battery, while the battery was in a discharged condition. In order to measure the potentials of the two external cells, terminals were inserted and soldered into the intercell connectors. These intercell connections are shown in Fig. 2. Epoxy seals were used to make modifications leak tight. Charge–discharge cycling data and impedance data were collected on these modified batteries.

The cycling and impedance data on the Yuasa NP 10-6 6 V 10 Ah batteries were obtained with a Solartron, 1470 Multichannel Battery Test System controlled by Solartron

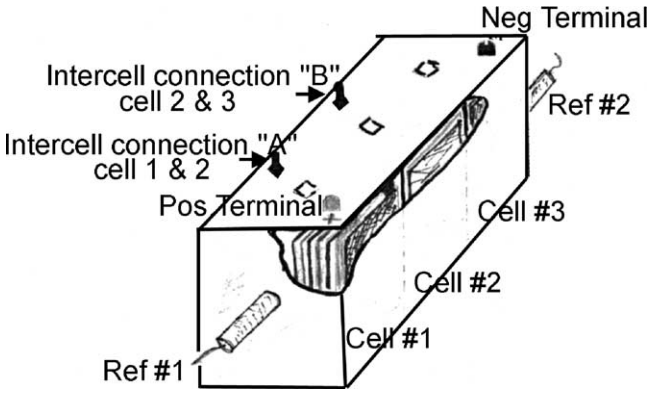

Fig. 2. Cutaway drawing of Yuasa NP 10-6 battery with reference electrodes.

Cell Test™ software. The impedance spectroscopy sweeps were conducted from 65 kHz to 0.65 Hz at amplitude of 5 mV. Measurements were made at 10% state-of-charge (SOC) intervals, both on charging and discharging with the batteries in an upright orientation. Constant current charging and discharging was performed at four different currents: 250, 500 mA, 1 and 2A.

Additional impedance data with respect to the reference electrodes was taken on the Yuasa NP 10-6 6 V 10 Ah batteries using a Solartron 1280B Electrochemical System controlled by Corrware and Zplot software. The first step in these measurements was the charging of the entire battery, via the positive and negative terminals (see Fig. 2) so that all three cells were uniformly charged. A constant current charge of 2.5 A was followed by a constant voltage float charge at 7.5 V. Charge was terminated when the current dropped to 0.1 A. Cells 1 and 3 were individually discharged at a constant current of 1.9 A at 10% SOC increments down to a cutoff voltage of 1.7 V. The impedance measurements were made in a three-terminal configuration with the following arrangements for the electrode connections:

For measurements with respect to the cell 1: Solartron working electrode was connected to battery positive terminal; Solartron reference lead 2 was connected to ref. #l; Solartron counter electrode and reference lead 1 were connected to intercell connection "A".

For measurements with respect to the cell 3: Solartron working electrode was connected to intercell connection "B"; Solartron reference lead 2 was connected to ref. #2; Solartron counter electrode and reference lead 1 were connected to battery negative terminal.

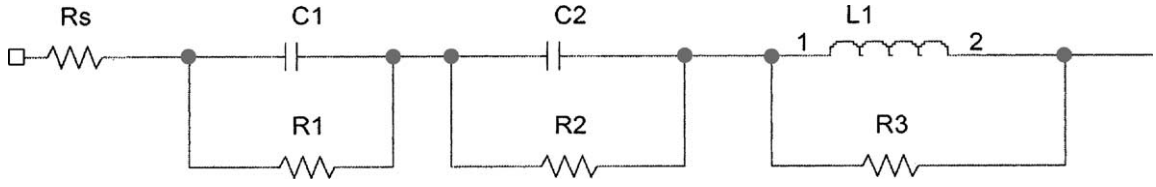

Fig. 3. Equivalent circuit model of lead–acid batteries.

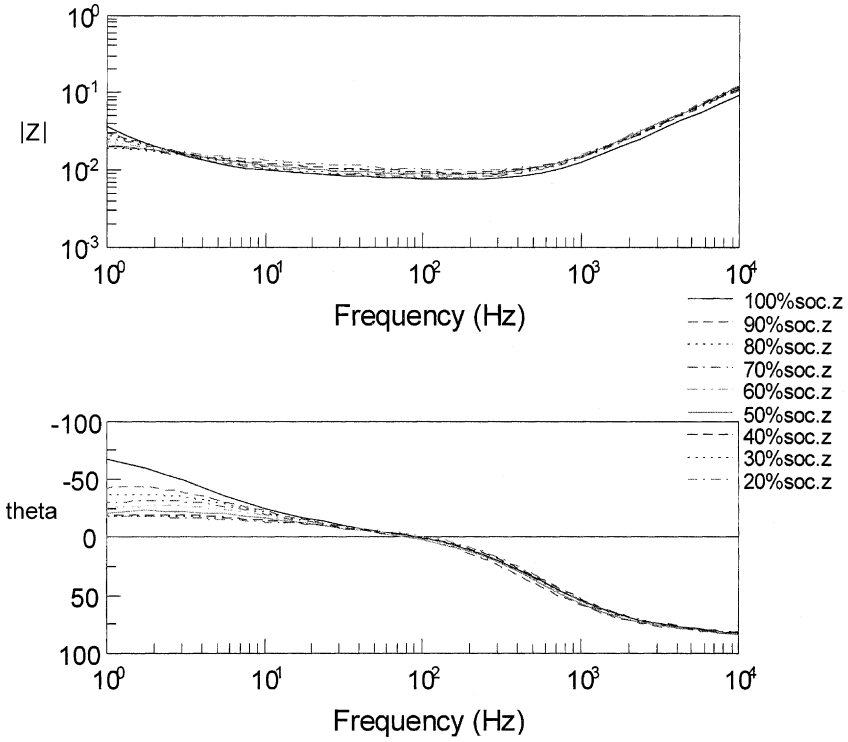

Fig. 4. Bode plots of magnitude and phase of impedance at −20 °C (Exide US6TMF).

The impedance data on the Exide (US) Military US6TMF 12 V 100 Ah batteries (see Fig. 1b) were taken using a Solartron 1280B Electrochemical System controlled by Corrware and Zplot software. These measurements were made over a frequency range of 1 Hz to 10 kHz in galvanostatic mode at a constant current that resulted in a 10 mV voltage amplitude applied to the battery. Data reduction was performed using Zview software. This software employs complex non-linear least squares analysis to curve fit data to prescribed equivalent circuit models. The impedance measurements were made at different temperatures at different SOCs in the case of the US6TMF batteries. The batteries were placed in a Tenney TU Jr. oven and feedthroughs used to contact the batteries. All measurements were made in a four-terminal configuration to circumvent the problem of contact resistance.

3. Modeling/analysis of impedance data

The equivalent circuit model used to fit the impedance data is shown in Fig. 3. The bulk series resistance of the battery is modeled by the series resistance, R_s and the two electrodes are modeled by parallel resistor–capacitor networks. A parallel inductor–resistor network is used to model the high frequency part of the impedance characteristics. The Bode plots for the impedance magnitude and the phase angle are shown in Fig. 4 for the Exide US6TMF batteries at −20 °C at different states of charge (SOCs) in the range of 100–20% SOC.

The Bode plots for magnitude and phase of impedance at 40 °C are shown in Fig. 5. The variation of the equivalent circuit parameters with SOC and temperature are shown in Fig. 6. The bulk series resistance R_s is seen to increase as the battery becomes progressively more discharged as expected since the electrolyte resistance will decrease as its pH decreases upon battery discharge. Furthermore, the bulk series resistance is also observed to increase as the temperature of the battery decreases again as expected. The

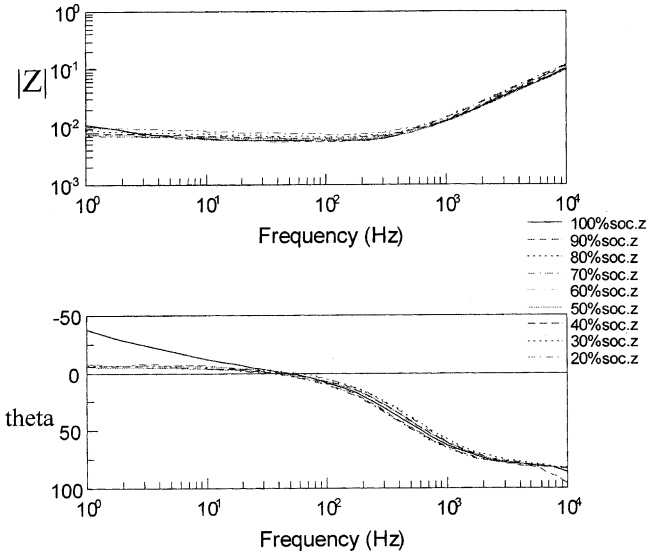

Fig. 5. Bode plots for magnitude and phase of impedance at 40 °C (Exide US6TMF).

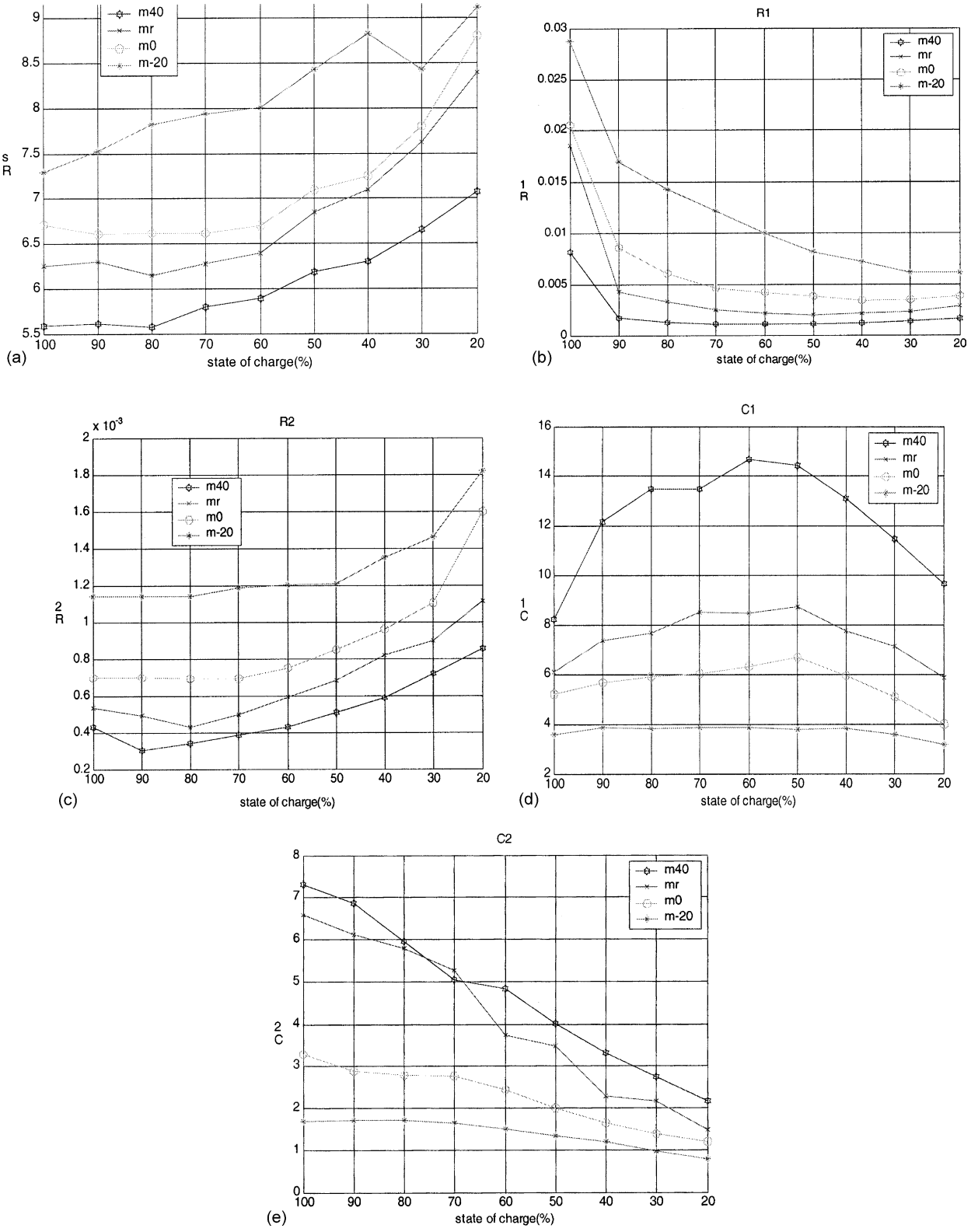

Fig. 6. (a) Variation in R_s with SOC and temperature (Exide US6TMF); (b) variation in R_1 with SOC and temperature (Exide US6TMF); (c) variation in R_2 with SOC and temperature (Exide US6TMF); (d) variation in C_1 with SOC and temperature (Exide US6TMF); (e) variation in C_2 with SOC and temperature (Exide US6TMF).

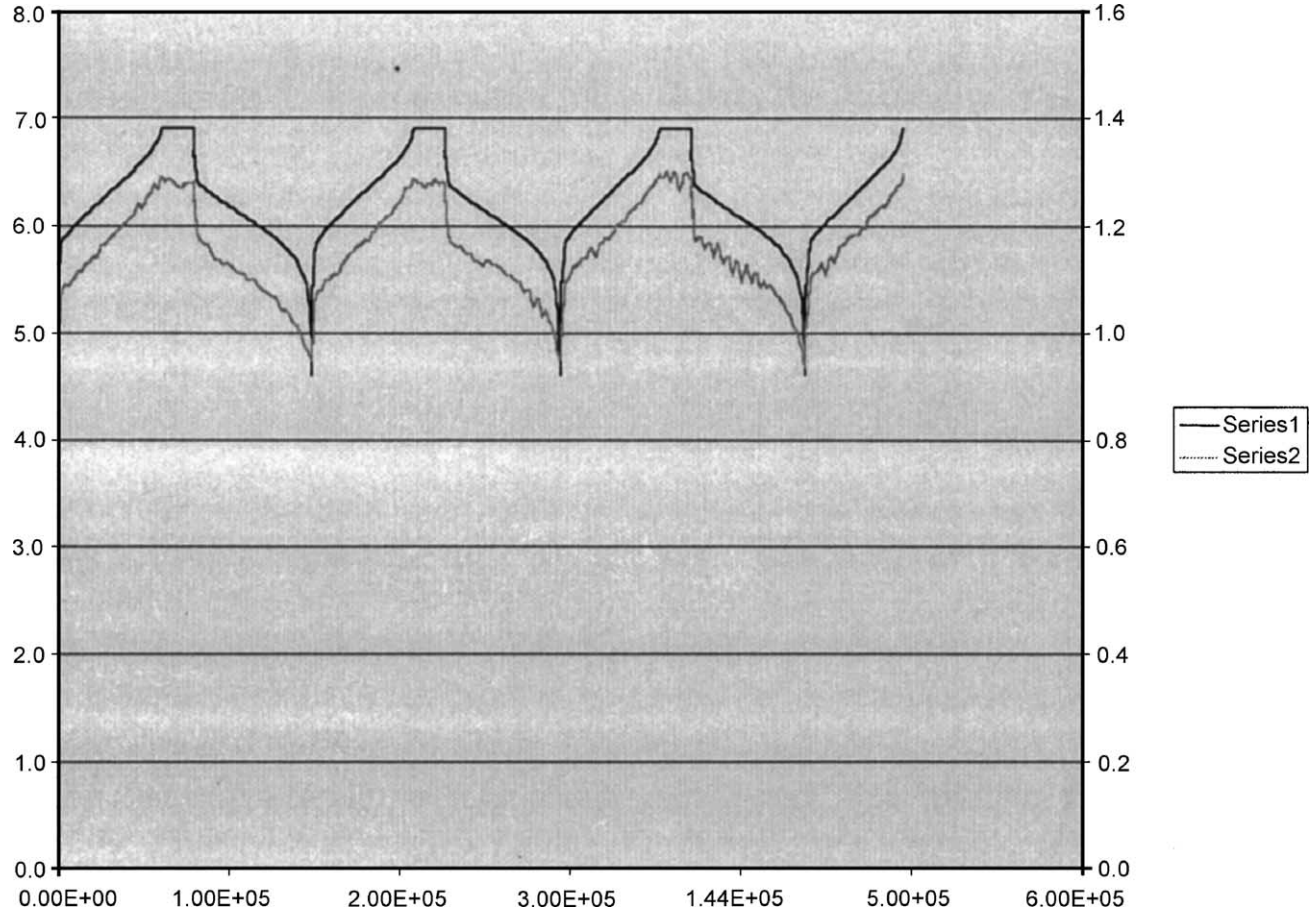

Fig. 7. Cell 1 voltage and voltage of positive electrode vs. ref. #1 electrode for several charge–discharge cycles (500 mA constant current charge and discharge).

reaction resistance RI is seen to drop dramatically as the battery is initially discharged from a full SOC but then flattens out below about 50% SOC. However, the reaction resistance R_2 is observed to be quite flat for the first 40% of the discharge cycle followed by a steady increase beyond 60% SOC. At low temperatures the C_1 capacitance remains quite flat but at higher temperatures it rises to peak at about 50% SOC as the battery is discharged from a fully charged state and then decreases as the battery SOC continues to decrease.

The C_2 capacitance for the Exide US6TMF battery was observed to continuously decrease as the battery SOC decreased with a more significant variation seen at higher temperature.

Fig. 7 shows the charge–discharge cycle curves for the Yuasa NP 10-6 6 V 10 Ah batteries measured for cell 1 and for the positive electrode versus reference electrode for several constant current (500 mA) charge–discharge cycles.

Fig. 8 is a similar plot for the negative electrode versus ref. #2 electrode for cell 3. While the cell voltage and voltage of the positive electrode versus ref. #l electrode are seen to track together in cell 1, the voltage variation is much smaller for the negative electrode versus ref. #2 electrode in cell 3 with a dramatic decrease of voltage when the cell becomes completely discharged.

The dynamic impedance properties for the NP 10-6 type battery illustrated in Fig. 1a, are shown in Fig. 8a–d [reference voltages during charge and discharge are shown in Figs. 7 and 8]. The data illustrates the characteristics of charging discharging at a high current regime of 2 A and a low current regime of 0.25 A. Data at 1 and 0.05 A were also taken and the results are intermediate between the extremes shown in the illustration. Fig. 8a shows the dynamic impedance during charge at 0.25 A, Fig. 8b the data for the discharge at 0.25 A, Fig. 8c the dynamic impedance at the 2.0 A charge, and Fig. 8d the data for the discharge. Charging was current limited, modified constant potential to 6.8 V. During the constant potential fart of the charge regime, the amount of capacity inputted was a function of the charge rate, since full charge transfer had occurred during the constant current portion of the regime at the low charge rates. For example, at 2 A approximately 50% of the total charge transfer occurring the constant voltage period. Whereas, at the 0.25 A charge rate, less than 5% of the total charge transfer occurred during the constant potential part of the charging regime.

On comparing Fig. 8a and c, the effect of charge rate on circuit modeling becomes clear. At high charge rates the large out of phase component of the impedance indicates a large surface capacitance which appears to instantly disappear on the onset of discharge. Please note there was a 15 min relaxation period between these charges and discharges.

As indicated earlier, impedance measurements were made with respect to the reference electrodes for the Yuasa NP 10-6 6 V 10 Ah batteries. The Bode and Nyquist plots for these

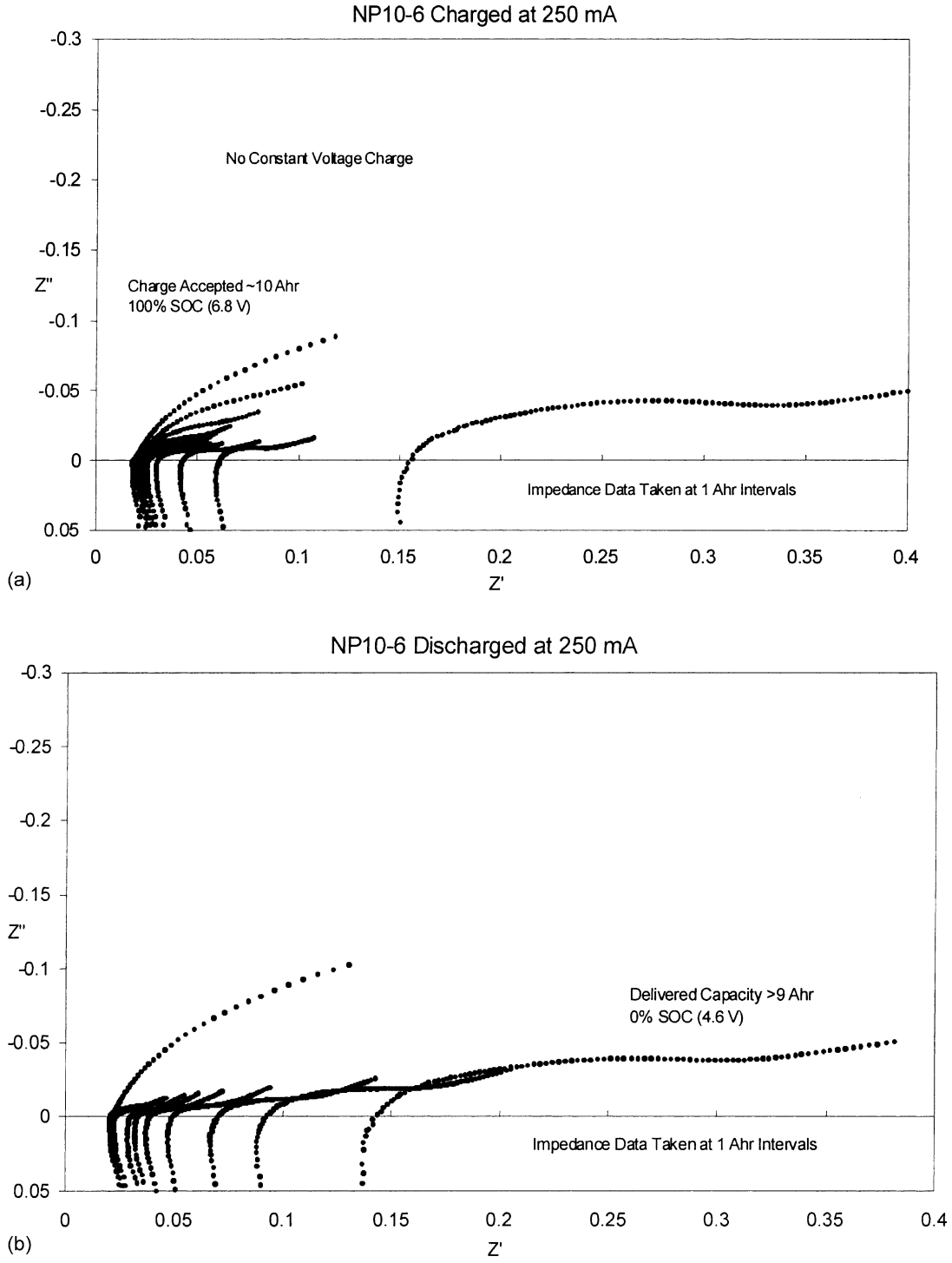

Fig. 8. Cell voltage and voltage of negative electrodes vs. reference electrode for several charge–discharge cycles (500 mA constant current charge and discharge). Dynamic impedance characteristics of NP 10-6 batteries during: (a) charge (0.25 A); (b) discharge (0.25 A); (c) charge (2.0 A); (d) discharge (2.0 A).

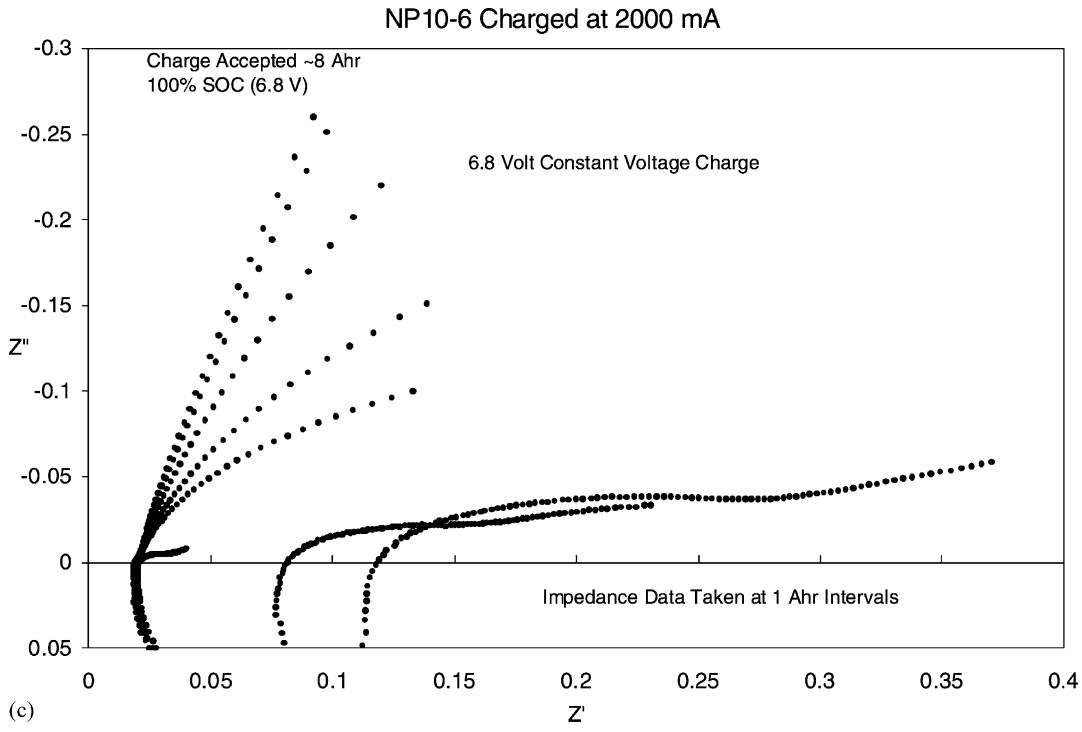

(c)

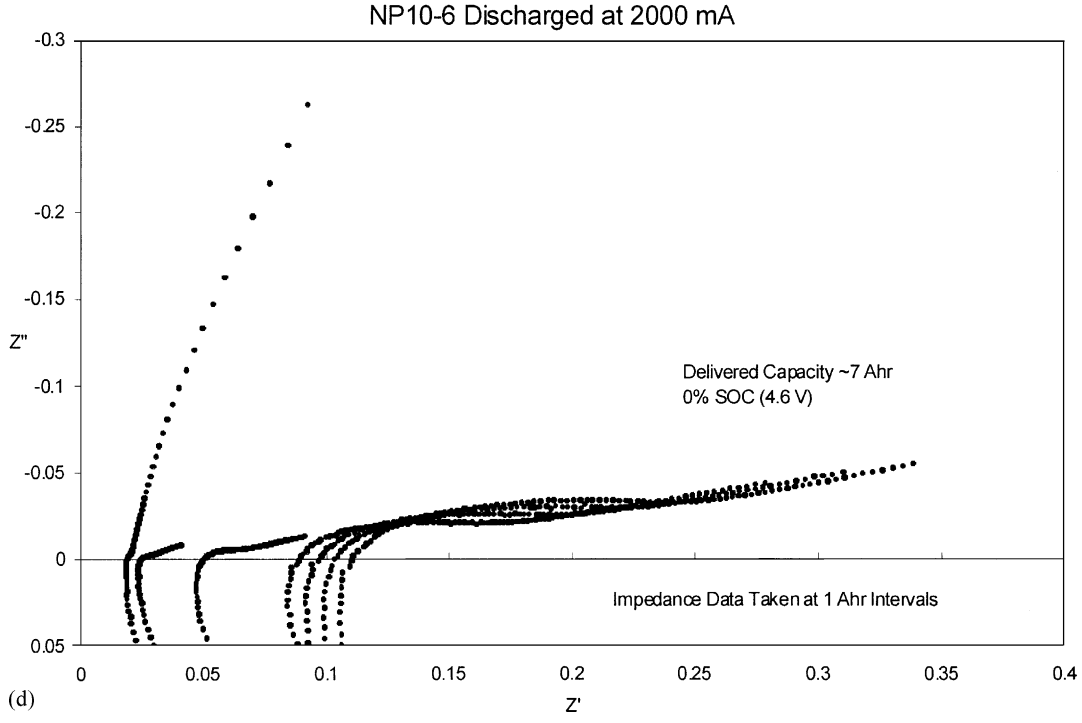

(d)

Fig. 8. (*Continued*).

measurements are shown in Figs. 9–13 as functions of battery SOC.

The equivalent circuit parameters as a function of SOC derived from these data are shown in Figs. 13a–e. From these figures, it is observed that the individual cell parameter values for cells 1 and 3 track together.

4. Discussion and conclusions

1. The extensive data taken with the NP 10-6 design appears to be typical for mid-size VRLA batteries and confirms the preliminary modeling reported at the 7th ELBC. The ac impedance methods of studying the

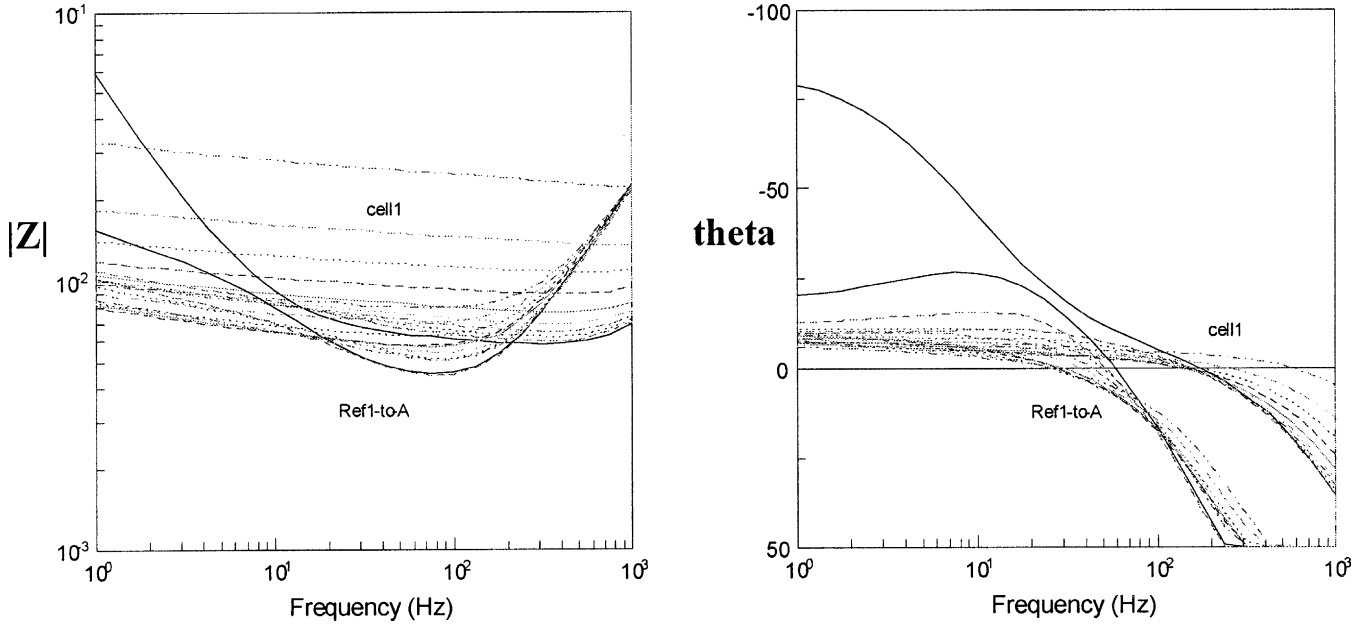

Fig. 9. |Z|, phase vs. frequency for cell and ref. #1-to-A.

electrochemical dynamics, combined with fuzzy logic modeling, enable the convenient solution to the derivation of an equivalent circuit and the design of state-of-charge and state-of-health testing and control devices. Studies on the effect of charge rate in current limited modified constant potential charging, indicate significant differences in the electrochemical double-layer as a function of charge rate in the CC portion. When the charge rate was 0.5 A, almost the entire charge transfer occurred in the CC period. When the CC charge rate was 2.0 A, almost the entire charge was transferred under CP control, and the double-layer capacitance was much greater at the end of charge. This might be useful in using this type design for electronic filtering purposes.

2. The testing and data obtained with the US6TMF (12 V, 100 Ah tank battery) indicate similar overall electrochemical dynamics obtained with the smaller VRLA cells and batteries reported previously as well as in this paper. This should lead to the development of greater understanding of the effect of temperature and cycling on performance and the development of a simple equivalent circuit model and control device.

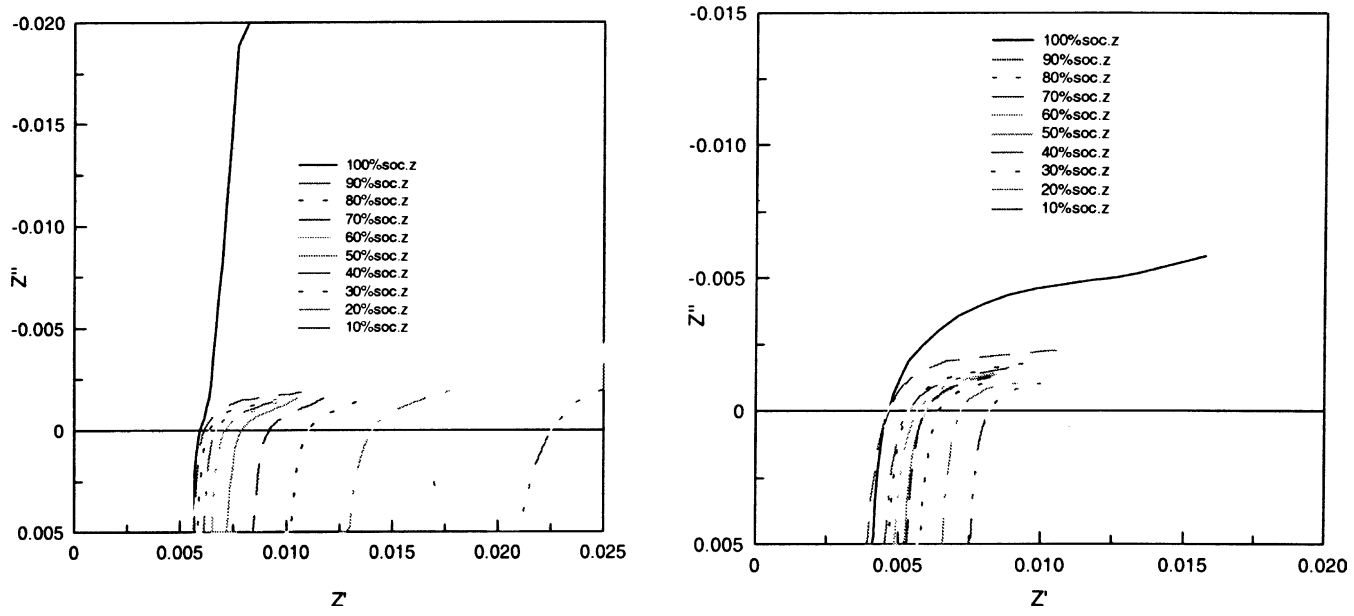

Fig. 10. Nyquist plot for cell 1 (left) and ref. #1-to-A (right).

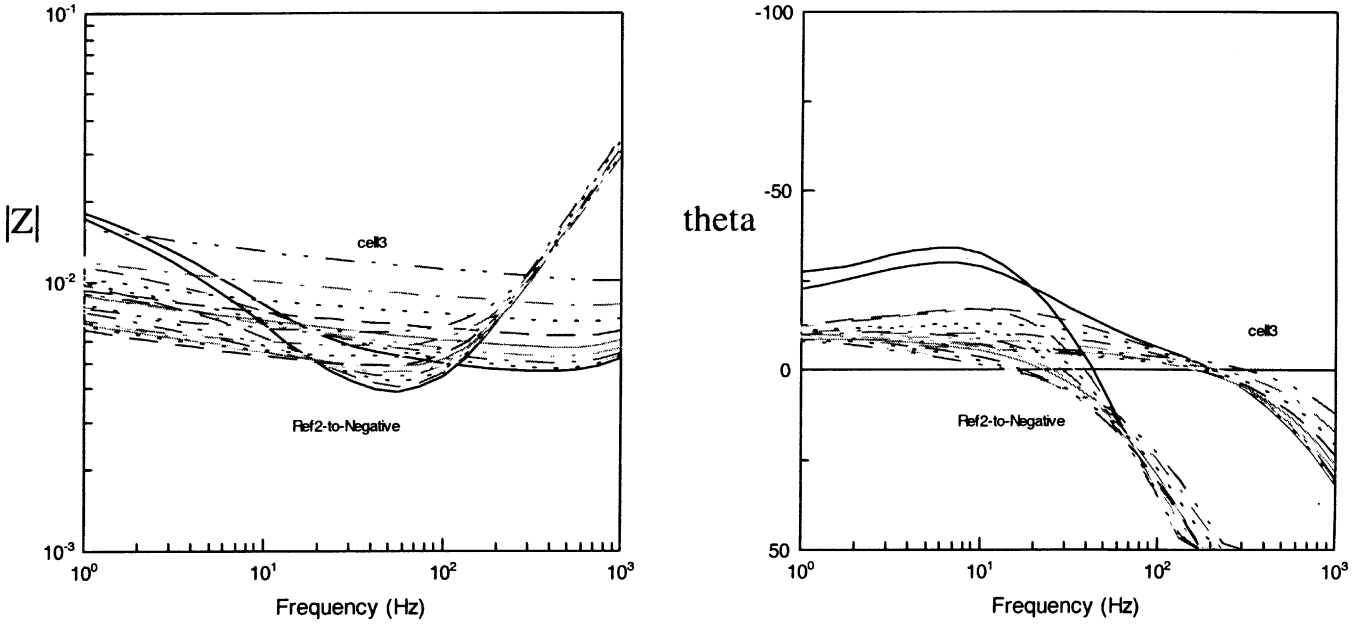

Fig. 11. |Z|, phase vs. frequency for cell 3 and ref. #2-to-negative.

3. Although it is not discussed in this presentation, in order to save space, data taken with a 12 V battery stack of cylindrical "D"-size lead–acid batteries, confirms the model earlier reported [6] with individual cells. This type pack is now in use in an external defibrillator and other high reliability equipment, where prediction of performance is critical to the use.
4. The Yuasa NP 10-6 battery and similar designs from various manufacturers are extensively used in a variety of applications and orientations. The data reported in this paper was taken in the upright position on previously cycled batteries. We plan to correlate old and new data with cycle life and positional variation.
5. The combination of fuzzy logic modeling and electrochemical impedance spectroscopy has been previously utilized by the authors to design devices for state-of-charge and state-of-health determinations for the Li/SO_2 and Ni–MH systems [1]. We believe that the approach and data reported in this paper can lead to similar devices for most lead–acid designs and applications.

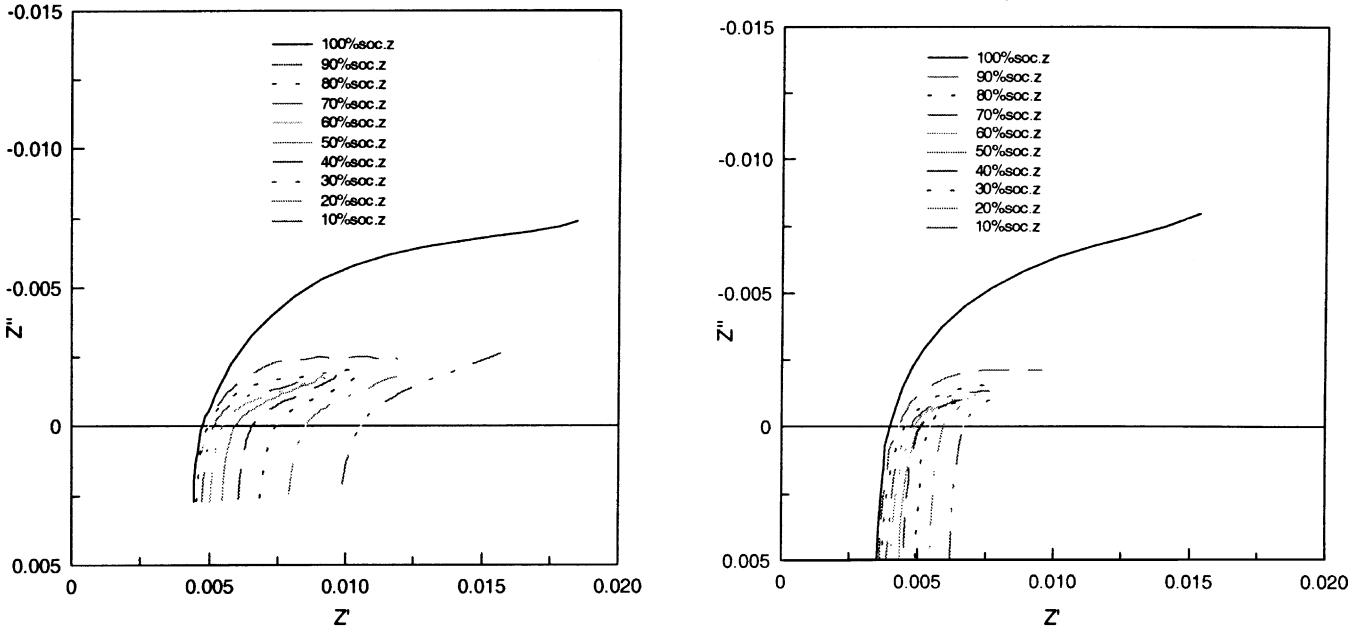

Fig. 12. Nyquist plot for cell 3 (left) and ref. #2-to-negative (right).

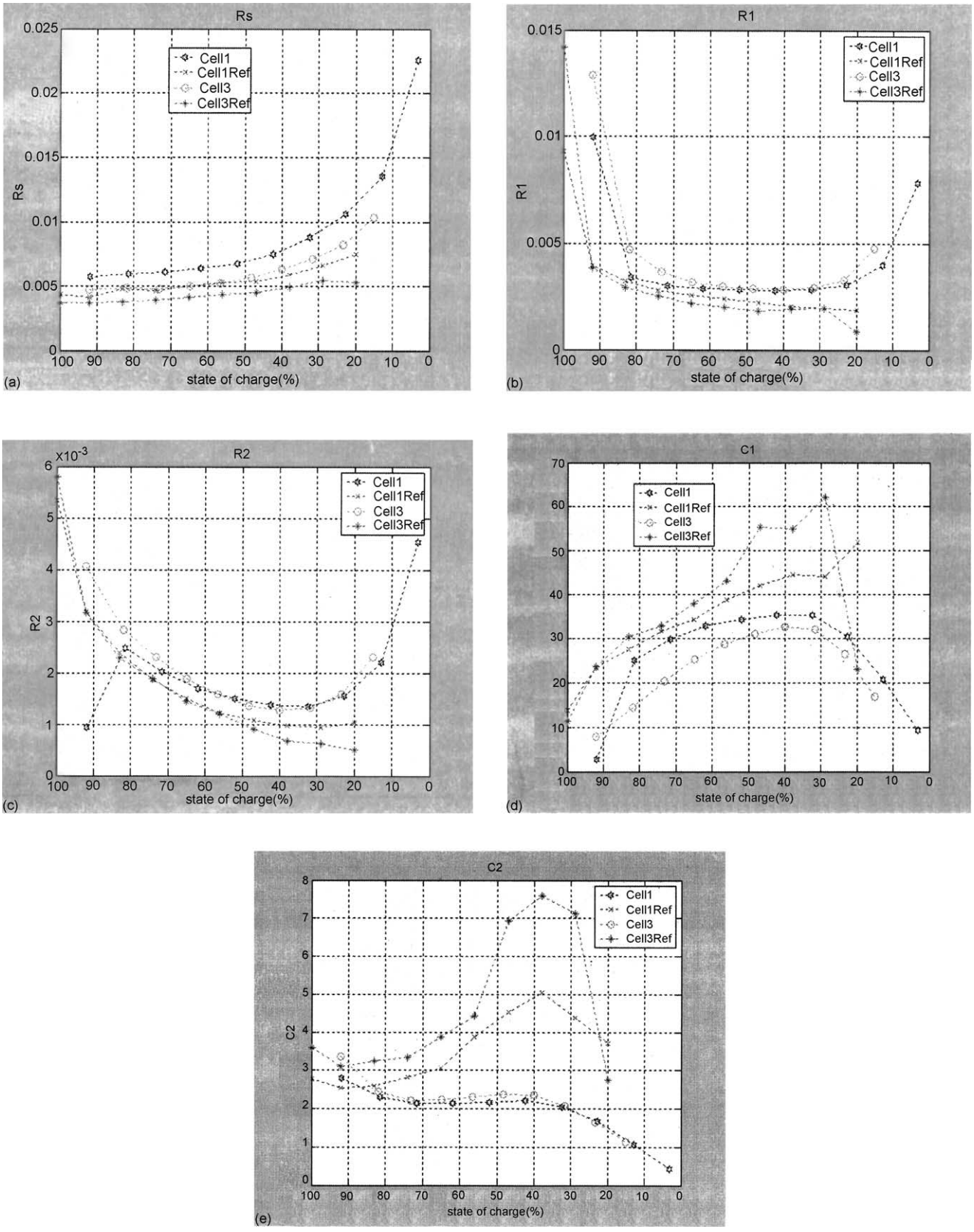

Fig. 13. (a and b) Variation of R_s and R_1 with SOC (Yuasa NP 10-6); (c) variation of R_2 with SOC (Yuasa NP 10-6); (d and e) variation of C_1 and C_2 with SOC (Yuasa NP 10-6). Cell1Ref stands for the ref. #l-to-A in cell 1, and Cell3Ref stands for the ref. #2-to-negative in cell 3.

Acknowledgements

Various activities discussed in this report were supported by a number of projects and institutions at the different groups and locations. We appreciate their support and guidance. US Army for TACOM Project at Villanova University (Contract DAAE07-01-C-L035). Yuasa Inc. [now EnerSys Inc.] (Mr. Frank Chiacchio) for donation of cell, components and batteries to Rutgers University and UMDNJ-Robert Wood Johnson Medical School.

References

[1] E. Karden, S. Buller, R.W. De Doncker, A frequency domain approach to dynamical modeling of electrochemical power sources, Electrochim. Acta (2002) 2347–2356.
[2] E. Karden, S. Buller, R.W. De Doncker, A method for measurement and interpretation of impedance spectra for industrial batteries, J. Power Sources 85 (2000) 72–78.
[3] F. Huet, A review of impedance measurements for the determination of state-of-charge and state-of-health of secondary batteries, J. Power Sources 70 (1998) 59–69.
[4] K. Champlin, K. Bertness, A fundamentally new approach to performance analysis using DFRA/DFIS technology, in: Proceedings of the 22nd International Telecommunications Engineering Conference, Paper 19.3, 2000, pp. 348–355.
[5] A.J. Salkind, C. Fennie, P. Singh, T. Atwater, D. Reisner, Determination of state-of-charge and state-of-health of batteries by fuzzy logic methodology, J. Power Sources 80 (1999) 293–300.
[6] A.J. Salkind, P. Singh, et al., in: Proceedings of the 22nd IPSS, Manchester, England, April 2001.
[7] V. Viswanathan, A.J. Salkind, J.J. Kelley, J.B. Ockerman, Effect of state-of-charge on impedance spectrum of sealed cells. Part II. Lead–acid, J. Applied. Electrochem. 25 (1995) 729–739.
[8] R. Biagetti, I. Baeringer, F. Chiacchio, A. Cannone, J. Kelley, J. Ockerman, A.J. Salkind, in: Proceedings of the Intelec, Vancouver, Canada, September 1994.
[9] P. Singh, et. al., in: Proceedings of the 201st Electrochem Society, Philadelphia, PA, May 2002.
[10] P. Singh, A.J. Salkind, C. Fennie, D. Reisner, Modeling of square pulse and impedance analysis of D size lead–acid cells, in: Proceedings of the 7th ELBC Poster Presentation, Dublin, Ireland, 19–22 September 2000.
[11] A.J. Salkind, T. Atwater, Investigation of small sealed lead–acid batteries, in: Proceedings of the 7th ELBC Poster Presentation, Dublin, Ireland, 19–22 September 2000.